

# HIGH ENERGY ELECTRON RADIOGRAPHY EXPERIMENT RESEARCH BASED ON PICOSECOND PULSE WIDTH BUNCH

Quantang Zhao, Shuchun Cao, Rui Cheng, Xiaokang Shen, Zimin Zhang<sup>#</sup>,  
Yongtao Zhao, IMP, CAS, Lanzhou 730000, China  
Wei Gai, ANL, Argonne, IL 60439, USA  
Yingchao. Du, THU, Beijing, 100084, China

## Abstract

A new scheme is proposed that high energy electron beam as a probe is used for time resolved imaging measurement of high energy density materials, especially for high energy density matter and inertial confinement fusion. The first picosecond pulse-width electron radiography experiment was achieved by Institute of Modern Physics (IMP), Chinese Academy of Sciences (CAS) and Tsinghua University (THU), based on THU Linear electron accelerator (LINAC). It is used for principle test and certifying that this kind of LINAC with ultra-short pulse electron bunch can be used for electron radiography. The experiment results, such as magnifying factor and the imaging distortion, are consistent with the beam optical theory well. The 2.5  $\mu\text{m}$  RMS spatial resolution has been gotten with magnifying factor 46, without optimization the imaging lens section. It is found that in the certain range of magnifying factor, the RMS spatial resolution will get better with bigger magnifying factor. The details of experiment set up, results, analysis and discussions are presented here.

## INTRODUCTION

The technique of charged particle radiography [1] has been developed and proved with 800 MeV protons at LANSCE of Los Alamos National Laboratory (LANL), as a diagnostic to study dynamic material properties under extreme pressures, strain and strain rate. The high spatial resolution and high energy proton microscopy also developed at ITEP and FAIR [2-4]. LANL used 30 MeV electrons to radiograph thin static and dynamic eRad with picosecond pulse-width electron bunch has been achieved by IMP, CAS and THU. The experiment objects. The spatial resolution of their imaging system is 100  $\mu\text{m}$  in both x and y directions [5]. A principle test of is based on the THU Thomson X-ray scattering source. The LINAC consists of RF photocathode injector and s-band accelerating tube. The RF photocathode injector provides 3 MeV, very low emittance and picoseconds pulse-width electron bunches. The highest beam energy of the LINAC is 50 MeV.

<sup>#</sup> zzm@impcas.ac.cn

## THE ERAD EXPERIMENT SETUP

In the eRad experiment, the beam energy is 46.3 MeV, bunch charge is about 100 pC, the emittance is about 2 mm-mrad, the beam spot size is about 3 mm, the bunch length is about 1 ps and the beam momentum divergence is less than 1%. The lens consists of two triplets. For simplicity, the lens section is not designed purposely. The quadrupoles for imaging are provided by the old ones, which have been used for focusing the beam in the Thomson scattering X-ray experiment.

The sketch of eRad experiment is shown in Fig. 1. The target vacuum cell and YAG and mirror vacuum cell are added. The electromagnetic quadrupole lens section consists of two triplets. The maximum of the magnetic field gradient is 12 T/m.

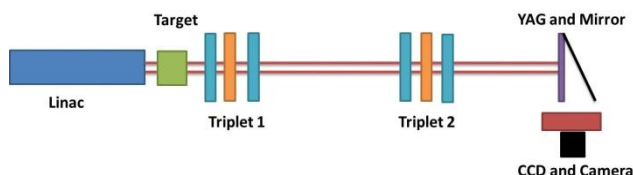


Figure 1: the sketch of the eRad based on THU linac.

The samples are electron microscopy grids, placed on the object plane. Four kinds of grids are installed in the target cell. They include 50 meshes square nickel (Ni) grid, 200 meshes square gold (Au) grid, 200 meshes square copper (Cu) grid and 75 meshes hexagon Cu grid. They are all in 25 microns thickness and 3 mm diameter. They are installed in a column, and can be moved up and down by a stepper motor. The samples pictures are shown in Fig. 2 (a). In the experiment, a criterion is set, if the 200 meshes square Au grid is imaging clearly, it is considered that the parameters of the lens section is suitable for imaging, shown in Fig. 2 (b). The other experiments can be taken under these conditions.

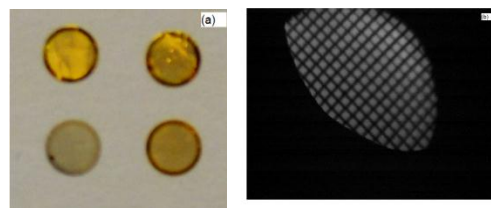


Figure 2: the picture of the samples (a) and the image of 200 mesh Au grid (b).

## EXPERIMENT RESULTS AND ANALYSIS

Based on the imaging criterion mentioned above, the other three samples, 50 meshes square Ni grid, 75 meshes hexagon Cu grid and 200 meshes square Cu grid, are well radiographed. The images are shown in Fig. 3.

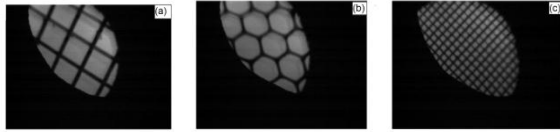


Figure 3: The images of the samples (a) 50 meshes Ni grid (b) 75 meshes Cu grid (c) 200 meshes Cu grid.

### Electron Optical Analysis

The parameters of imaging lens section can be decided by the imaging criterion mentioned above. The voltages and currents supplied for the quadrupoles are recorded under imaging conditions, by which the magnetic gradient parameters of the two triplets can be calculated.

The lens section transfer matrix can be calculated by Transport [6]. The first order beam optical transport is also studied based on the above parameters. The envelope plot of the imaging lens section is shown in Fig. 4.

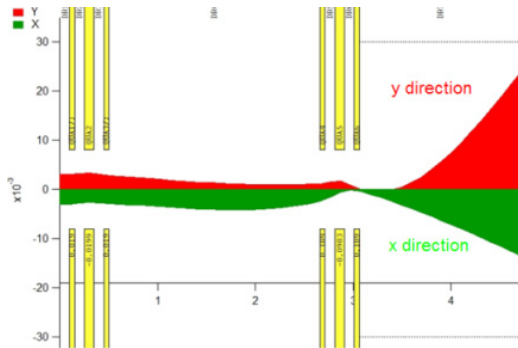


Figure 4: The envelope of the imaging lens section.

In the ray trace plot, shown in Fig. 5, five points in the object plane are assumed to emit five beam on each point, with different emitting angle, 0.1, 0.2, 0.3, 0.4, 0.5 mrad individually. From the first order beam optics theory, the position on the imaging plane of each point depends on the first order transport matrix, shown in formula (1).

$$\begin{aligned} x_{\text{image}} &= R_{11}x + R_{12}\theta \\ y_{\text{image}} &= R_{33}y + R_{34}\psi \end{aligned} \quad (1)$$

From the transfer matrix of the lens section, the value of  $R_{34}$  is bigger than  $R_{12}$ , so in the ray trace, the emitting angle will influence more in y direction than in x, which is identical with formula (1), shown in Fig. 5. In y direction the image point will blur more than in x direction.

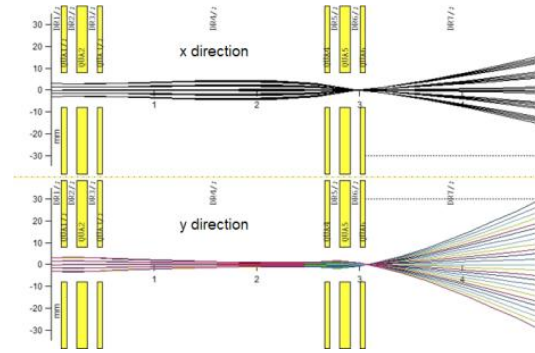


Figure 5: the ray traces plot of the imaging lens section.

### Magnifying Factor Analysis

The image of 50 meshes square Ni grid is chosen for analysis. One grid was used for magnifying factor analysis, shown in Fig. 6. Before the experiment, the CCD and camera was calibrated by a rule, which placed on the imaging plane. It is shown that one pixel is 8.125um. So in the Fig.6, the  $|AB| = \sqrt{|OA|^2 + |OB|^2}$ , OA and OB can be obtained by the pixel coordinates of point O, A and B. The distance of AB in the image is 2193.75 um. The distance of AB of the sample is just one pitch, equals to 500 um. Assuming the magnifying factor is M, there is  $M=4.38$ . So the magnifying factor in X direction is 2.48 and in Y direction is 3.68. Compared with the lens section transfer matrix, the  $R_{11} = -2.30927$  is X direction magnifying factor and the  $R_{33} = -3.89845$  is the Y direction magnifying factor. The experiment results are consistent with the calculated results well.

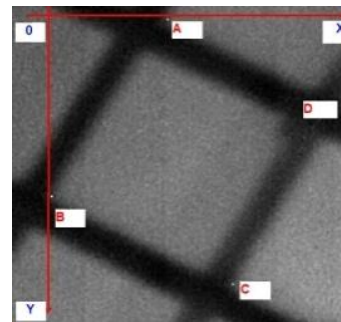


Figure 6: One grid of the 50 meshes Ni grid image.

In Fig. 6, it is shown that the image of square sample is not square because of the different magnifying factor in X direction and Y direction and the x direction and y direction of the sample grid is placed not parallel with the x direction and y direction of beam, which was certified by the simulation with beam tracking code PARMELA [7]. In the simulation, the maximum beam energy is 46.3 MeV and the minimum is 45.9 MeV, the momentum divergence is 1% and the beam distribution is in Gauss distribution. The grids on object plane are shown in Fig. 7 (a). With the same lens section parameters mentioned above, the final beam distribution is shown in Fig. 7 (b) on the image plane. The simulation results are well explained the image distortion.



**REFERENCES**

- [1] C L Morris, N S P King, K Kwiatkowski, F G Mariam, F E Merrill and A Saunders. Charged particle radiography, Rep. Prog. Phys. 76 (2013) 046301.
- [2] Karen E. Kippen, Robert D. Fulton, Eric Brown, William T. Buttler, Amy J. Clarke, et al. AOT & LANSCE Focus: Proton Radiography Facility, LA-UR-13-24376.
- [3] A.V. Kantsyrev, A.A. Golubev, V.I. Turtikov et al. ITEP PROTON MICROSCOPY FACILITY, IEEE Pulsed Power Conference (PPC), 2013.
- [4] F. E. Merrill, A. A. Golubev, F. G. Mariam, et al. PROTON MICROSCOPY AT FAIR. AIP Conference Proceedings 1195, (2009) 667.
- [5] Frank Merrill, Frank Harmon, Alan Hunt, et al. Electron radiography, Nuclear Instruments and Methods in Physics Research B 261 (2007) 382–386.
- [6] PSI Graphic Transport Framework by U. Rohrer based on a CERN-SLAC-FERMILAB version by K.L. Brown et al.
- [7] Lloyd M. Young. Parmela, LA-UR-96-1835 Revised May 23, 2005.